Available online at www.sciencedirect.com
ScienceDirect
Cement & Concrete Composites 29 (2007) 465–473
Cement & Concrete Composites
www.elsevier.com/locate/cemconcomp

Investigation of the strengthening effect of DFRCC applied to plain concrete beams

S.K. Shin, J.J.H. Kim, Y.M. Lim *

School of Civil and Environmental Engineering, College of Engineering, Yonsei University, Seoul 120-749, Republic of Korea

Received 10 July 2006; received in revised form 14 February 2007; accepted 15 February 2007
Available online 6 March 2007

Abstract

One of the most important characteristics of Ductile Fiber Reinforced Cementitious Composite (DFRCC) is its strain hardening behavior up to 5–6% *strain* under tensile loading. In this study, the strengthening effect of DFRCC, applied to the tension region of plain concrete beams, is both numerically and experimentally examined. More specifically, 10%, 20%, and 30% of the beam height are replaced with DFRCC to measure the strengthening effect of the composite beam. From four-point bending tests and numerical simulations, the load–deflection behaviors are investigated and compared. To assess the effect of ultimate tensile strength, strain capacity and strain hardening slope of DFRCC, numerical simulations are carried out with DFRCC strain capacities ranging from 1% to 5%. From these studies, it is shown that DFRCC significantly contributes to the deflection capacity, load carrying capacity and failure modes of concrete beams.

Keywords: Ductile fiber reinforced cementitious composite; Strain hardening; Strain capacity; Strengthening effect; Numerical model

1. Introduction

Multitudes of concrete structures were constructed during the 1960s and 1970s. After 30–40 years of service life, time has come to make a decision whether to repair or replace many of these concrete structures. For the successful repair of structures, structural health evaluation, methodology of repair, and selection of repair materials are three important factors [1,2]. Many different materials have been developed for the purpose of repairing deficient structures. They range from Portland cement-based materials to polymer-based materials. However, polymeric materials have been utilized in limited applications as a repair material for concrete structures because, in part, of concerns about the long-term compatibility between the concrete substrate and the repair material.

Compatibility between substrate and repair material is the most important factor in selection of repair material. Cement-based materials are suitable for repairing concrete structures due to their mechanical and physical properties (e.g. coefficient of thermal expansion, fracture energy, permeability), as well as other important considerations such as cost, availability, and constructability [3–6].

Recently, different types of cement-based composites have been developed to control mechanical properties, such as elastic modulus, ultimate tensile strength, and strain capacity. This is possible through characterization and engineering of the three main phases of the composite: matrix, fiber and fiber–matrix interface. For this reason, composites can be tailored for unique applications by maximizing their mechanical properties and characteristics. Recently, Ductile Fiber Reinforced Cementitious Composites (DFRCC) with moderate elastic modulus, moderate tensile strength, and high tensile strain capacity have been developed based on micro mechanical models [7–11]. One of the most promising areas of application of this material is using the material to the repair of concrete structures.

The present paper investigates the importance of the ductility of DFRCC when it is used as repair material on concrete structures under flexural loading. A lattice-type

* Corresponding author. Tel.: +82 2 2123 2796; fax: +82 2 364 5300.
E-mail address: yunmook@yonsei.ac.kr (Y.M. Lim).

0958-9465/$ - see front matter © 2007 Elsevier Ltd. All rights reserved.
doi:10.1016/j.cemconcomp.2007.02.005

model was developed to study damage in concrete and cement-based composites [12–15]. At this stage, strain hardening behavior of DFRCC has been implemented in the model and the simulation results (Group B beams) are compared with experimental data (Group A beams). Composite beams are also numerically simulated with DFRCC having different strain capacities to investigate the effect of ultimate tensile strength and strain hardening slope (Group C and D beams).

2. Numerical modeling

2.1. Background of numerical method

Lattice models have been widely used for simulation of brittle failure of materials [16–19]. In the most basic case, crack growth is modeled by removing (from the mesh) the element with the highest stress-to-strength ratio. The computation is repeated until failure in the complete mesh is obtained. The fracture is based on the maximum tensile stress that occurs in the outermost fiber of a frame element due to moment and normal force at nodes i and j as shown:

$$\sigma = \frac{\beta}{(1-\Omega)}\left(\frac{F}{A} + \alpha\frac{\max(|M_i|,|M_j|)}{W}\right), \quad (1)$$

where F is the axial force in the frame element, M_i and M_j are the bending moments at nodes i and j of the frame element, respectively. The parameter A is the section area of frame element with width b and depth h, and W is the element section modulus ($bh^2/6$). Ω is a damage parameter which is initially set to zero for all elements; $\Omega = 1$ corresponds to element removal from the lattice (i.e. complete damage). The constant α is a parameter to control the influence of flexure on the fracture and β is a parameter for scaling the element effective stress to global stress levels. The significance of parameters α and β was discussed in Refs. [20–22].

The lattice model is based on the iteration of linear elastic lattice behavior when nonlinearity is introduced. Once an element is removed from the system, the solution is repeated linearly to get another point on the load–deformation curve. As will be shown later, the model can realistically describe the cracking patterns. The model's main drawback, however, is its highly irregular macroscopic stress–deformation relation particularly in the post-peak region.

Cement-based materials such as concrete and DFRCC always fail due to tensile cracking at the microlevel. In this study, therefore, the ADLE (Axial Deformation Link Element) model [12–15] was introduced to investigate the fracture behavior of the materials. This model considers only axial deformation between two neighboring points. At each load stage, the effective stress σ acting in each element is computed according to Eq. (1) when $\alpha = 0$. The ADL element with the highest ratio $R = \sigma/\sigma_f$ experiences a fracture event when $R \geqslant 1.0$, where σ is the axial stress in the element and σ_f is the tensile strength of the material. Element internal forces associated with this change are released, with both the element and system stiffness matrices reformed. To model the macroscopic nature of the material and fracture process better, the stiffness of fracturing elements was gradually reduced via damage parameter Ω depending on the component type. The ADLE model adopts the fictitious crack model with post-peak softening curve to overcome the weakness of a lattice type model as mentioned earlier. This model reveals a realistic stress–strain response similar to that observed experimentally for concrete material.

2.2. Constitutive relations of concrete and DFRCC

The softening behavior of the concrete is implemented through the stress-crack separation relations in order to arrive at a mesh–objective representation of fracture [23]. It is assumed that the stress–strain relation for the elements is linearly elastic up to its tensile strength of the phase considered, followed by softening. Hence, the elastic parameters required to establish the first part of the relation are elastic modulus (E) and tensile strength (f_t). The inelastic parameters associated with the softening part of the curve are fracture energy (G_F) and the shape of the stress–separation curve. When these parameters are specified, a complete constitutive relation can be established for each individual element based on its length. Unlike concrete materials, however, DFRCC exhibits tensile strain-hardening characteristics. A constitutive relation for an ordinary DFRCC is shown in Fig. 1.

The tensile stress increases linearly up to first cracking strength f_t, after which DFRCC undergoes strain-hardening up to the ultimate tensile strength $\beta_s f_t$. The ultimate tensile strength parameter β_s can change according to the characteristics of DFRCC. During strain-hardening, multiple micro-cracks are successively formed and finally those cracks become nearly equally spaced in parallel. In the strain-softening region, transmitted tensile stress decreases after strain-hardening. During strain-softening, the "strain" is not uniquely defined, but depends on gauge length. Deformation at this stage is more appropriately described by crack opening displacement, and begins to localize in the transition from uniform deformation field (multiple cracking deformation) to the crack opening displacement of a single crack.

The first step of numerical procedure is data input for mesh generation and material property assignment. For the mesh generation step, axial deformation link elements (ADLE) are generated and each element is assigned with material properties such as elastic modulus, first cracking strength, ultimate tensile strength, and fracture energy [23,24]. In this material property assignment process, material properties vary about their mean values with 10% coefficient of variation (c.o.v). This deviation of material properties is provided by Monte Carlo simulation using a normal distribution. From the previous research, c.o.v has a slight effect on the response. The predicted response

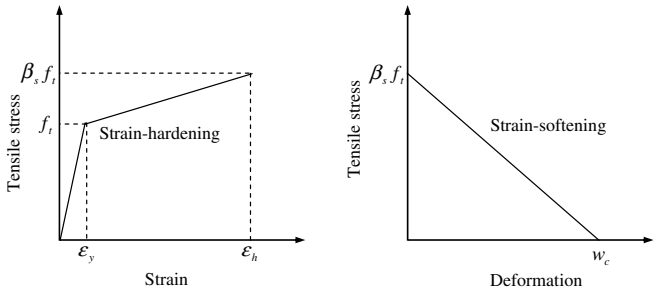

Fig. 1. Constitutive relationship of DFRCC.

of c.o.v 10% is well matched with experimental result [13,14,23].

The calculated initial stiffness matrices are assembled and incremental loadings are applied. After obtaining the displacements at the nodes, the strain in each element is calculated. If the new strain value indicates that the element status has changed in this iteration, the new status is assigned to the element and the stresses are calculated based on the updated status. After updating the status of all elements, the residual force vector at all free nodes is assembled together with the reaction force vector at the supports. If the ratio between the norm of the residual vector and the norm of the reaction vector satisfies the prescribed tolerance, the program will record the required information for the current increment and then move to the next increment. Otherwise the iteration procedure is activated. Fig. 2 shows the flow chart of the computer program.

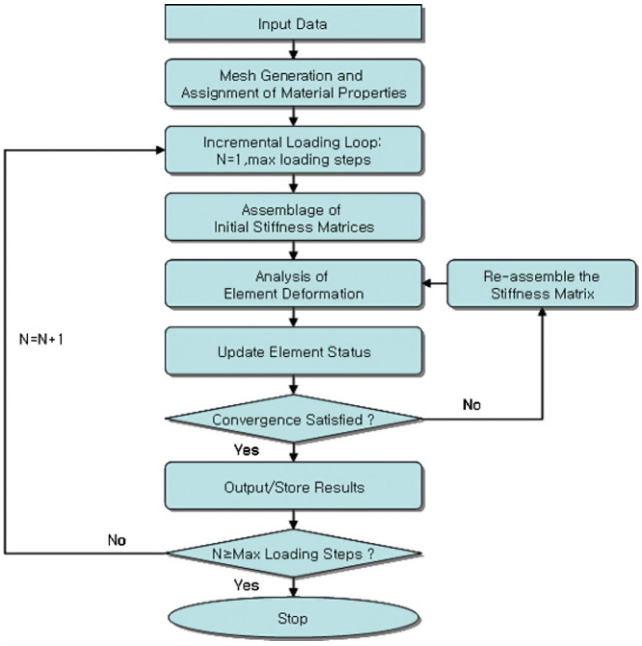

Fig. 2. Flow chart of the computer program.

3. Verification of developed numerical method on DFRCC

3.1. Direct tension test

To demonstrate the feasibility of the developed numerical program to DFRCC, a direct tension test specimen is simulated. The dimensions of the test specimen are 76.2 mm × 254.0 mm × 38.1 mm. The lengths of horizontal elements, vertical elements, and diagonal elements are 3.81 mm, 4.70 mm, and 6.05 mm, respectively. The number of total elements is 1629. The test specimen and numerical model are depicted in Fig. 3. The material properties used in this simulation are same as those of an experiment [1]: the elastic modulus $E = 20.0$ GPa, the first cracking strength $f_t = 2.5$ MPa, and the ultimate tensile strength is 5.0 MPa ($\beta_s = 2.0$). Stress–strain curves for DFRCC are shown in Fig. 4. The numerical results agree with those of the experiment in tension, strain-hardening, and localization zone as an upper limit.

The crack patterns associated with the marked points on the typical response (A–C in Fig. 4) are shown in Fig. 5. At point A where micro-cracks initiate, most of the ADL elements are still in elastic region, and the others are in strain-hardening region. At point B, ADL elements in strain-hardening region are greater in number and distributed throughout the whole specimen. In the real situation, multiple cracking is observed in DFRCC specimen. As the loading process is advanced, a number of ADL elements go into strain-softening region. In the end, the specimen comes to failure. It can be found that the load–deflection

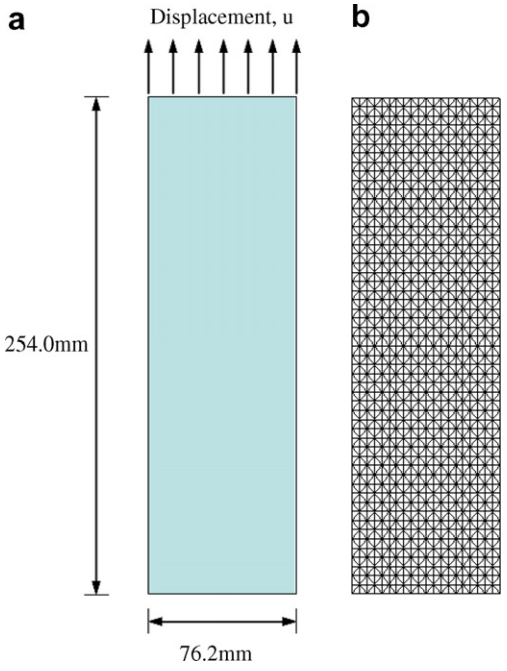

Fig. 3. (a) Specimen configuration used in direct tension simulation. (b) Mesh layout.

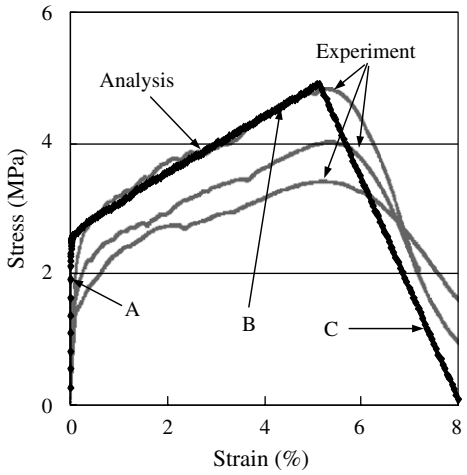

Fig. 4. Experimental and simulated response of DFRCC under direct tension.

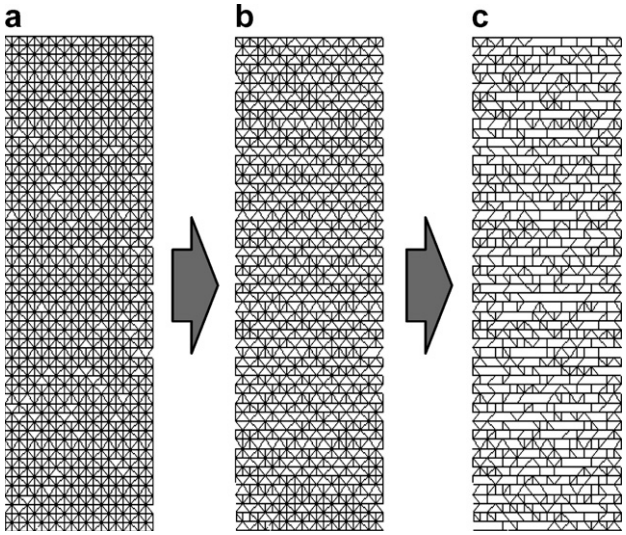

Fig. 5. Predicted cracking patterns of DFRCC under direct tension: (a) point A, (b) point B, and (c) point C.

curve and the failure mechanism in both cases, simulation and test, are quite similar.

3.2. Bending test

In the following section, a three-point bending set-up is used to investigate the behavior of DFRCC. Fig. 6 schematically illustrates the test set-up, specimen size and loading configuration [1]. The material properties are same as those used in the direct tension test, and the constitutive relation of DFRCC is the same as well.

Fig. 7 shows the experimental and analytical load–deflection response for bending test of DFRCC specimen. The numerical results are almost identical to those of experiment. The first cracking load of DFRCC is around 4.2 kN and the peak load is around 10 kN at deflection of 4–5 mm. Fig. 8 shows the micro-cracking for loading

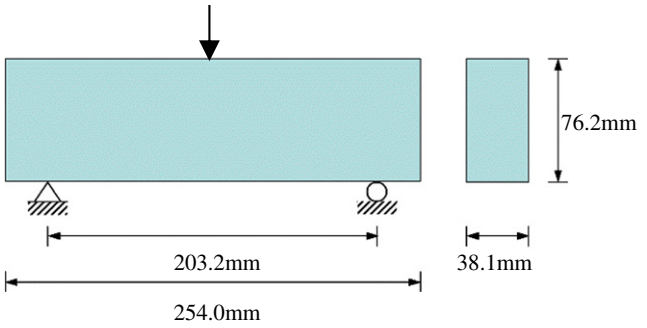

Fig. 6. Specimen configuration used in bending simulation.

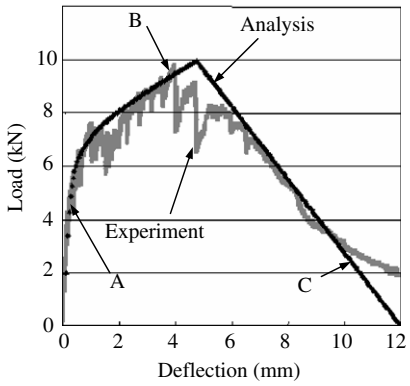

Fig. 7. Experimental and simulated response of DFRCC under three-point bending.

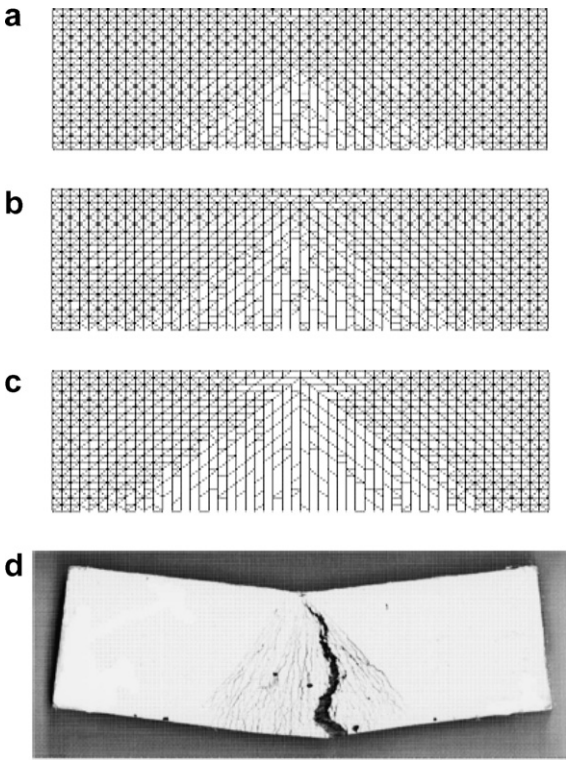

Fig. 8. Failure mechanisms of DFRCC loaded in three-point bending: (a) point A, (b) point B, (c) point C of the numerical model, and (d) experiment.

steps A, B, and C. In this figure, the elements in strain-hardening and strain-softening region have been removed from the mesh. The plotted mesh only includes the undamaged elements. Fig. 8a illustrates that some micro-cracks are initiated at the tensile region. At point B, the number of ADL elements belonging to strain-hardening region has increased. The crack propagates towards the loading point of the beam. At point C, the number of cracking elements has further increased, and the beam finally fails. This cracking procedure agrees with the experimental results (refer to Fig. 8d) [1].

4. Effects of DFRCC ductility

4.1. Experimental program

4.1.1. Scheme of experimental work

Fig. 9 shows the test beam cross-sections with DFRCC thicknesses of 0%, 10%, 20%, and 30% of the beam height (beams A0, A10, A20, A30, respectively). For comparison, a control beam (A0) which is not strengthened with DFRCC is tested. The beams are applied with displacement-controlled load with loading rate of 0.005 mm/s. The inner dimensions of formwork used in this experiment are 10 cm wide, 10 cm high and 40 cm long, manufactured with 2 cm thick acryl plates.

4.1.2. Materials and specimen preparation

The cement used in this experiment is type I ordinary Portland cement of Larfarge Halla Cement Company (Korea). For fiber, specially coated PVA fiber of Kuraray Company (Japan) is used. Material properties of the fiber are shown in Table 1. The length and diameter of the PVA fibers are 1.27 cm and 39 μm, respectively. With silica sands which are much finer than the fine aggregates generally used in concrete, the workability of DFRCC is improved by minimizing the difficulties of PVA fiber distribution. The use of silica sand also helps to control the toughness of the composite and enhance bond friction at the matrix–fiber interface by filling up the pores. Fly ash and super-plasticizer (SP) are used to lower the W/C ratio and to improve workability during concrete casting. The type of SP is ADVA100. In addition, methyl cellulose (MC) from S Company of Korea is used to enhance the workability of the mixed materials, to avoid material segregation, and to improve the fiber distribution during mixing.

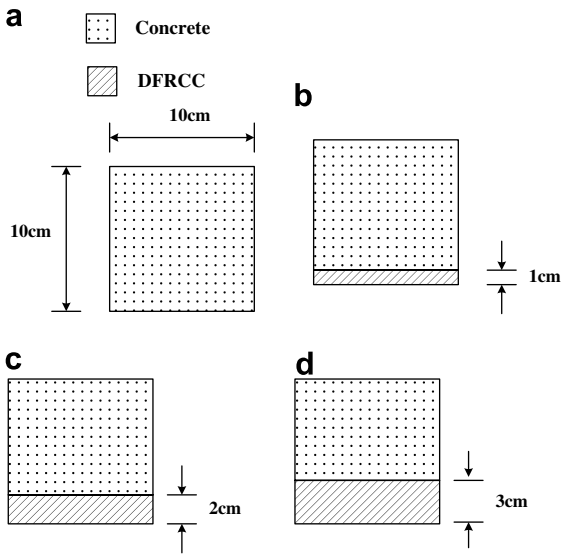

Fig. 9. DFRCC thickness: (a) 0%, (b) 10%, (c) 20%, and (d) 30% of the beam height.

Table 1
Mechanical properties of fiber

Diameter (μm)	Tensile strength (MPa)	Percentage of elongation (%)	Modulus of elasticity (GPa)	Specific gravity
39	1620	6	42.8	1.3

DFRCC was mixed with the following procedures. First, powder cement, fly ash, and fine aggregate are mixed uniformly in dry condition using a 20 l capacity rotary mixer for two or three minutes, followed by gradual addition of water. The liquefied MC and SP were sequentially added to the mix. The mixture with additives was maintained in a very diluted and uniform condition for about three minutes. After 3 min, the short fibers were evenly added into the mix and stirred for three minutes. DFRCC was put on a vibration table for about 20 s. Finally, DFRCC was casted on the prepared concrete beams. Fig. 10 shows photographs of the casted beams. After beams were casted, the open surface was covered with a wet paper towel to prevent drying shrinkage from occurring on the surface. The casted beams and frame were sealed with a plastic cover to prevent water loss. After 24 h, the beams were demolded and cured for 28 days under water. A total of 12 specimens were made. Table 2 shows the number of specimens prepared for each layer thickness of DFRCC.

For the four-point bending test of beams, MTS-810 with a 25-ton capacity is used. Fig. 11 shows an actual and schematic picture of the test set-up. The specimen is considered to have reached failure when the applied load reached below 30% of the maximum load, at which point the loading is stopped. In all of the result discussions, the maximum deflection value is equivalent to the deflection at 30% of the maximum load.

4.2. Behavior of concrete beam strengthened with DFRCC

In order to investigate the strengthening effect of DFRCC, numerical simulations are carried out for four-point bending specimens strengthened with DFRCC – 0%, 10%, 20%, and 30% of the beam height (beams B0, B10, B20, B30) and the results are compared to those

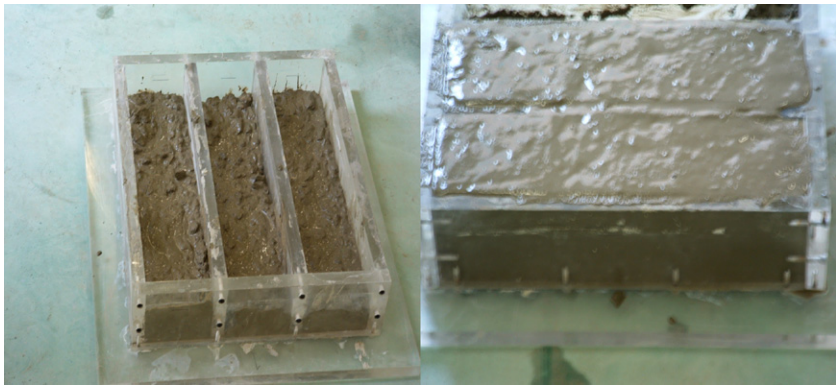

Fig. 10. Concrete beams strengthened with DFRCC.

Table 2
Number of specimens for each DFRCC thickness

Beam designations	DFRCC thickness	No. of specimens
A0	0	3
A10	10% (1 cm)	3
A20	20% (2 cm)	3
A30	30% (3 cm)	3

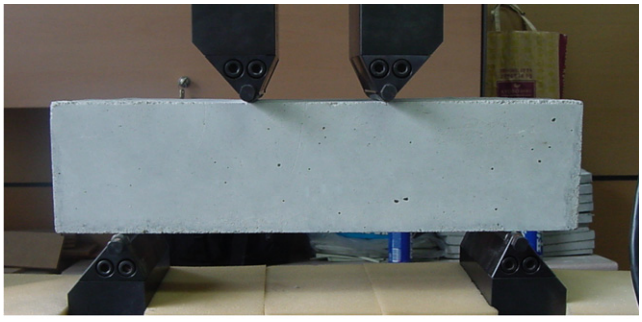

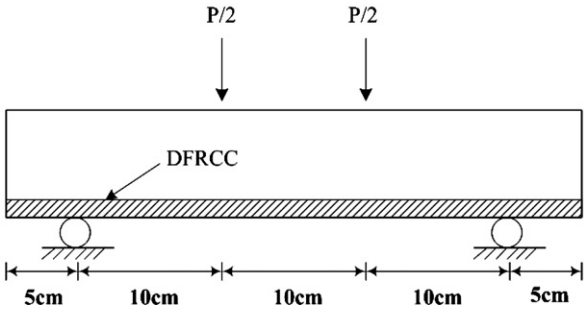

Fig. 11. Configurations of four-point bending test set-up.

obtained experimentally. The material properties such as modulus of elasticity, tensile strength, and ultimate strength of DFRCC are close to those of experimental work.

The results of simulation are shown in Fig. 12 together with the experimental results. The predicted load–deflection responses are very close to the experimental work up to the peak load. Especially, the trends of load–deflection curve in 10% and 20% are well matched with each other.

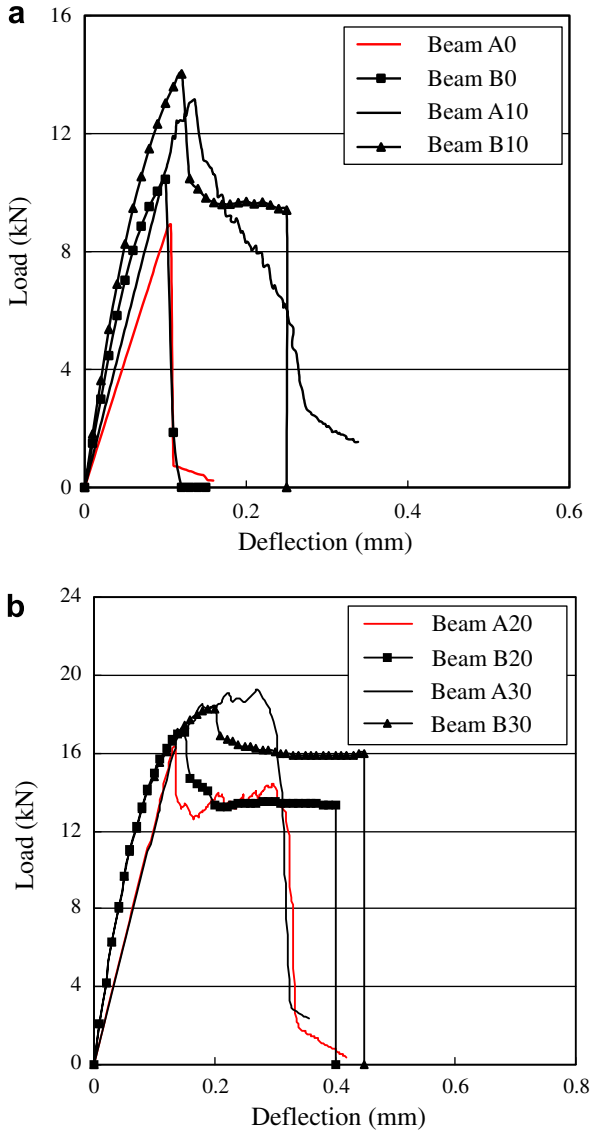

Fig. 12. Comparison of experiment and analysis for various thicknesses of DFRCC: (a) DFRCC thicknesses of 0%, 10% and (b) DFRCC thicknesses of 20%, 30% of the beam height.

As shown in this figure, the response of simulations is nearly linear up to about 60% of the peak load. At higher

loads, the response becomes nonlinear. Numerical simulations have more nonlinear behavior rather than experimental results. The higher degree of prepeak nonlinearity for the numerical simulations might be due to the use of a 10% c.o.v. in assigning the material properties for each element. After peak load, beam A0 and B0 (control beams) show a sudden drop, and fails in a brittle manner. On the other hand, DFRCC strengthened beams (beams A10, A20, A30, beams B10, B20, B30) exhibit significant degrees of ductility. The peak load of DFRCC strengthened beams is increased to the extent of 36–80%, and the maximum deflection is increased to the extent of 25–116% compared to the control beam. It is also shown from Fig. 12 that the size of the drop after peak is inversely related to the thickness of the DFRCC layer. The larger becomes the layer, the smaller the drop after peak load. This behavior is caused by the concrete part of the beam is fracturing in a brittle manner.

Moreover, DFRCC strengthened beams show much more stable fracture behavior with higher ductility and load carrying capacity than plain concrete beams. Observation of DFRCC strengthened beams reveals that cracks first occur in the concrete section, and subsequently propagate into the DFRCC section as distributed micro-cracks.

4.3. Effect of different constitutive relations of DFRCC

In the previous sections, the proposed numerical method is validated by comparative studies between experiments and analyses. From the results, simulations for the beam shown in Fig. 6 are conducted to assess the effect of ultimate tensile strength, strain capacity and strain hardening slope of DFRCC on the macro- and micro-mechanical behavior, such as load–deformation and cracking behavior. The DFRCC thickness is 10% of the beam height. Simulated beams are classified into two groups. For Group C beams shown in Fig. 13, DFRCC is assigned the same ultimate tensile strength of 5.0 MPa, whereas the strain capacity changes into 1%, 2%, 3%, and 5% with different strain hardening slope for each simulation (beams C1, C2, C3, C5, respectively). For another investigation, Group D beams are simulated. DFRCC is assigned the same strain hardening slope, whereas the strain capacity changes into

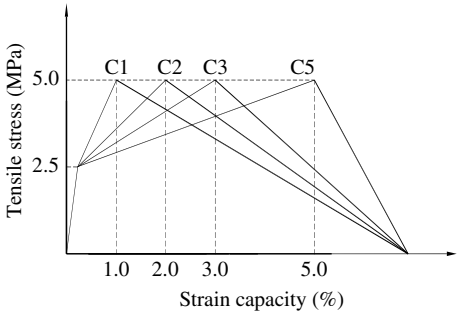

Fig. 13. Constitutive relations of DFRCC with different strain capacities for Group C beams.

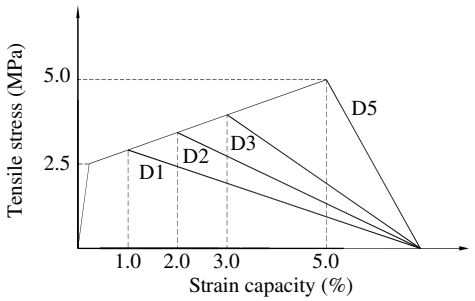

Fig. 14. Constitutive relations of DFRCC with different strain capacities for Group D beams.

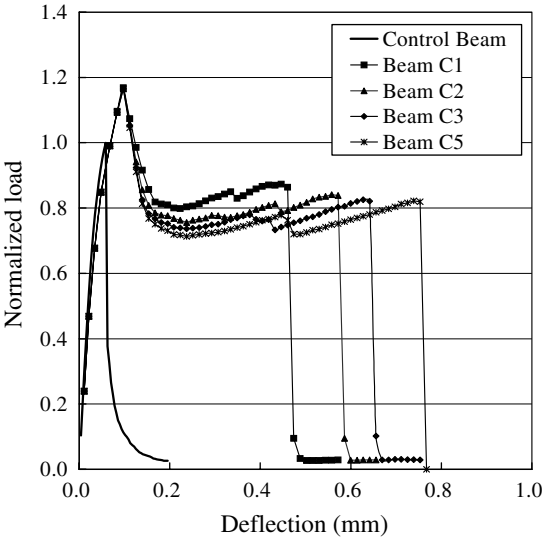

Fig. 15. Effect of different strain capacities on the normalized load–deflection response for Group C beams.

1%, 2%, 3%, and 5% for each simulation (beams D1, D2, D3, D5, respectively) as shown in Fig. 14. Accordingly, the ultimate tensile strength changes with strain capacity for the Group D beams.

The normalized load–deflection responses are depicted in Figs. 15 and 16 for the Group C and D beams, respectively. The peak loads of each beam are normalized by that of the control beam. It can be seen, for both groups, that the peak loads and associated deflections are the same regardless of the strain capacity of DFRCC. The peak loads and associated deflections increase by 17% and 66% for Group C and D beams compared to the control beam, respectively. It might be thought that strain capacity and strain hardening slope do not have an influence on the peak load when the strain capacity of strengthening material is higher than a certain value. The DFRCC strains associated with peak load are less than about 1%. The same strain hardening slope (Group D beams) results in the same reduction in load capacity after peak load. It is also noted that as the strain hardening slope becomes much stiffer (Group C beams), the reduction in load capacity becomes smaller. The simulation results for Group C and D beams

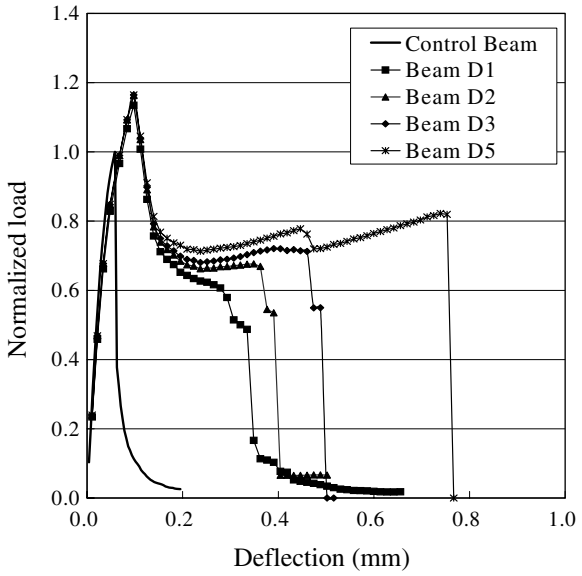

Fig. 16. Effect of different strain capacities on the normalized load–deflection response for Group D beams.

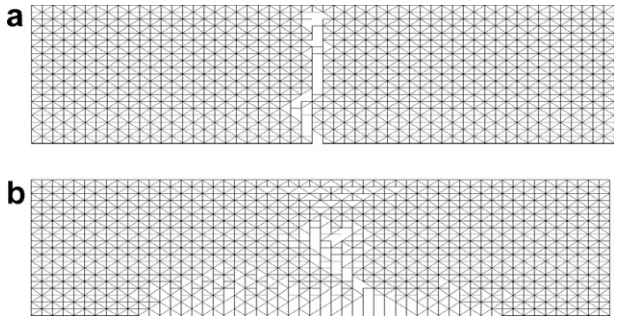

Fig. 17. Failure mechanisms of (a) control beam and (b) DFRCC strengthening beam (C1).

show that the load capacity after peak load is strongly influenced by the ultimate tensile strength.

Failure modes of the control beam and beam C1 are compared with each other at the instant when peak load is reached. In Fig. 17a, the control beam is failing by propagation of a major flexural crack from the bottom to the top of beams. Beam C1 has flexural cracks in the early loading stages with micro-cracks distributed in DFRCC region, but finally failure occurs due to concrete crushing when the concrete compressive strain exceeds its ultimate value (Fig. 17b). The other beams in Group C have the same failure mode as beam C1. The failure mode of Group D beams is also the same as Group C beams.

5. Concluding remarks

ADL element model is developed to predict the behavior of structures strengthened with Ductile Fiber Reinforced Cementitious Composites (DFRCC). The effect of strain capacity of DFRCC on a plain concrete beams was numerically and experimentally investigated. Following conclusions can be drawn through this study:

1. The predicted responses of DFRCC are compared to those obtained experimentally under direct tension and three-point bending tests. The developed numerical program, from these results, is found to be suitable for modeling the micro-cracking and macro-mechanical behaviors of DFRCC.
2. To investigate the effect of strain capacity of DFRCC material, a series of concrete beams which are supplemented with DFRCC in the tension region are tested and numerically simulated. DFRCC thickness is 0%, 10%, 20%, and 30% of the beam height. The peak loads of the composite beams are increased to the extent of 36–80%, and the associated deflections are increased to the extent of 25–116% compared to the control beam. The thickness of DFRCC is found to significantly contribute to the deflection capacity and flexural strength of the concrete beams.
3. In the beam simulations with different constitutive relations of DFRCC, the first cracking strength has an important influence on the peak load, while the post peak behaviors are strongly influenced by the ultimate tensile strength and strain hardening slope of DFRCC. Failure modes of control beam and DFRCC strengthened beams have shown that the strain capacity of DFRCC prevents brittle failure of the system. From the simulation results, DFRCC is required to be selected carefully to improve the flexural performance of concrete beams.
4. This study is mainly focused on the strengthening effect of DFRCC applied on plain concrete structures. It is anticipated that similar, yet less dramatic, improvements can be achieved when applying DFRCC to reinforced concrete members. However, the material selection should be carefully considered to achieve the target composite behavior of DFRCC and plain concrete.

References

[1] Lim YM. Interface fracture behavior of rehabilitated concrete infrastructures using engineered cementitious composite, Ph.D. Thesis, University of Michigan, Ann Arbor; 1996.
[2] Lim YM, Li VC. Durable repair of aged infrastructure using trapping mechanism of engineered cementitious composites. Cement Concrete Comp 1997;19(4):373–85.
[3] Kamada T, Li VC. The effect of surface preparation on the fracture behavior of ECC/concrete repair system. Cement Concrete Comp 2000;22:423–31.
[4] Li VC, Horii H, Kabele P, Kanda T, Lim YM. Repair and retrofit with engineered cementitious composites. Eng Fract Mech 2000; 65:317–34.
[5] Li VC, Wang S, Wu C. Tensile strain-hardening behavior of polyvinyl alcohol engineered cementious composite. ACI Struct J 2001:483–92.
[6] Bolander JE, Berton S. Simulation of shrinkage induced cracking in cement composite overlays. Cement Concrete Compos 2004; 26(7):861–71.

[7] Li VC. From micromechanics to structural engineering – the design of cementitious composites for civil engineering applications. JSCE J Struct Mech Earthquake Eng 1993;10(2):37–48.
[8] Kawamata A, Mihashi H, Kaneko Y, Kirikoshi K. Controlling fracture toughness of matrix for ductile fiber reinforced cementitious composites. Eng Fract Mech 2002;69:249–65.
[9] Kawamata A, Mihashi H, Fukuyama H. Material design of hybrid reinforced cementitious composites. In: Proceedings of the JCI international workshop on DFRCC, Takayama, Japan; October, 2002. p. 85–94.
[10] Mihashi H, Leite JPB, Yamakoshi S, Kawamata A. Controlling fracture toughness of matrix with mica flack inclusions to design pseudo-ductile fiber reinforced cementitious composites. Eng Fract Mech 2007;74:210–22.
[11] Badanoiu A, Holmgren J. Cementitious composites reinforced with continuous carbon fibres for strengthening of concrete structures. Cement Concrete Compos 2003;25:387–94.
[12] Lim YM, Kim MK, Shin SK, Heo WY. Numerical simulation for the interface behavior between the substrate and repair material based on fracture energy concept. In: Proceedings of APCOM 99, Singapore; December, 1999. p. 341–6.
[13] Lim YM, Kim MK, Shin SK. Interfacial fracture behavior in repaired concrete infrastructures. In: Proceedings of ICCE/7, Denver, Colorado, USA; July, 2000. p. 535–6.
[14] Lim YM, Kim MK, Li VC, Shin SK. Numerical simulation for quasi-brittle interface fracture in cementitious bi-material system. In: Proceedings of FramCos-4, Cachan, France; May–June, 2001. p. 73–80.
[15] Lim YM, Kim MK, Kim JHJ, Shin SK. Is ductility important for repair application? In: Proceedings of the JCI international workshop on DFRCC, Takayama, Japan; October, 2002. p. 199–208.
[16] Bolander JE, Saito S. Fracture analyses using spring networks with random geometry. Eng Fract Mech 1998;61:569–91.
[17] Cusatis G, Bazant ZP, Cedolin L. Confinement shear lattice model for concrete damage in tension and compression I. Theory. J Eng Mech 2003;129(12):1439–48.
[18] Cusatis G, Bazant ZP, Cedolin L. Confinement shear lattice model for concrete damage in tension and compression II. Computation and validation. J Eng Mech 2003;129(12):1449–58.
[19] Lilliu G, van Mier JGM. 3D lattice type fracture model for concrete. Eng Fract Mech 2003;70:927–41.
[20] Schlangen E, van Mier JGM. Experimental and numerical analysis of micromechanisms of fracture of cement-based composites. Cement Concrete Compos 1992;14:105–18.
[21] Schlangen E, van Mier JGM. Simple lattice model for numerical simulation of concrete materials and structures. Mater Struct 1992;25:534–42.
[22] Bolander JE, Shiraishi T, Isogawa Y. An adaptive procedure for fracture simulation in extensive lattice networks. Eng Fract Mech 1996;54(3):325–34.
[23] Ashraf RAM. Micromechanics of concrete behavior and progressive failure under static loading, Ph.D. thesis, University of Michigan, Ann Arbor; 1997.
[24] Hillerborg A, Modeer M, Petersson PE. Analysis of crack formation and crack growth in concrete by means of fracture mechanics and finite elements. Cement Concrete Res 1976;6:773–82.